

This is the postprint version of the following article: Gurruchaga-Pereda, J; Martinez-Martinez, V; Rezabal, E; Lopez, X; Garino, C; Mancin, F; Cortajarena, AL; Salassa, L. [Flavin Bioorthogonal Photocatalysis Towards Platinum Substrates](#). ACS Catalysis 2019, DOI: [10.1021/acscatal.9b02863](#)

This article may be used for non-commercial purposes in accordance with ACS Terms and Conditions for Self-Archiving.

Flavin Bioorthogonal Photocatalysis Towards Platinum Substrates

Juan Gurruchaga-Pereda,^{a,b} Virginia Martínez-Martínez,^c Elixabete Rezabal,^d Xabier Lopez,^{a,d} Claudio Garino,^e Fabrizio Mancin,^f Aitziber L. Cortajarena,^{b,g} Luca Salassa^{a,g*}

^a *Donostia International Physics Center, Paseo Manuel de Lardizabal 4, Donostia, 20018, Spain*

^b *CIC biomaGUNE, Paseo de Miramón 182, Donostia, 20014, Spain*

^c *Departamento de Química Física, Universidad del País Vasco, UPV/EHU, Apartado 644, Bilbao, 48080, Spain*

^d *Kimika Fakultatea, Euskal Herriko Unibertsitatea, UPV/EHU, Donostia, 20080, Spain*

^e *Department of Chemistry, University of Turin, via Pietro Giuria 7, Turin, 10125, Italy*

^f *Dipartimento di Scienze Chimiche, Università di Padova, via Marzolo 1, Padova, 35131, Italy*

^g *Ikerbasque, Basque Foundation for Science, Bilbao, 48011, Spain*

ABSTRACT

Catalytic reactions that use metal complexes as substrates, rather than catalysts, are nearly unknown. We recently demonstrated that certain flavins (FLs) are potent redox photocatalysts capable of converting Pt^{IV} anticancer prodrug complexes into Pt^{II} drugs in the biological environment. Herein, we investigate the mechanism of these artificial photocatalytic reactions employing four different free flavins, namely riboflavin (**Rf**), flavin mononucleotide (**FMN**), tetra-O-acetyl riboflavin (**TARF**) and lumiflavin (**Lf**), and the flavoprotein **miniSOG** (mini Singlet Oxygen Generator) together with a panel of Pt^{IV} substrates conveniently selected.

NMR, steady-state and time-resolved optical spectroscopy studies highlight that light activation of FLs in the presence of NADH as electron donor (pH 7–7.5) eventually leads to the generation of the reduced FLH⁻ species which catalyzes the Pt^{IV}-to- Pt^{II} conversion with turnover frequency (TOF) values ranging between 1.3 and 30 min⁻¹, and turnover number (TON) values reaching 500. Comparable catalytic efficiency is also found for reactions performed in cell culture medium. Density functional theory suggests that activation via reduction of the Pt^{IV} complexes may be influenced by H-bonding interactions between the FL catalyst and the metal substrate and confirm that both the isoalloxazine

and ribityl moieties of the FLs determine the catalytic efficiency of the process. The FMN-containing **miniSOG** is a less effective catalyst (TOFs < 5.6 min⁻¹) since the formation of the doubly reduced FMNH⁻ competes with an electron transfer reaction involving the protein matrix which quenches the FMN excited state to give a singly-reduced FMN⁻.

KEYWORDS

Photocatalysis, Flavins, Bioorthogonal catalysis, Platinum prodrugs, Chemotherapy, Photoactivation

INTRODUCTION

In catalysis, coordination and organometallic complexes typically act as catalysts to kinetically favor the conversion of organic substrates into added-value products. Recently, we subverted such a paradigm to conceive new approaches for the activation of metal-based anticancer prodrugs (**Figure 1**).¹⁻⁴ We demonstrated that flavins (FLs) can perform under light-irradiation as catalysts to prompt the transformation of transition metal substrates into their biologically active counterparts. In the presence of electron donors, flavin co-factors and certain flavoproteins are able to photoconvert Pt^{IV} precursors into cisplatin or carboplatin within biological environments, switching on the antiproliferative activity of the Pt^{II} drugs *in vitro*. This unconventional approach expands the substrate scope and versatility of bioorthogonal catalytic reactions currently available in drug development,^{1,5,6} potentially creating new uses for a myriad of inorganic biological agents that have been developed over the last decades as chemotherapeutics and antibacterial agents. The term bioorthogonal here refers to the capacity of these catalysts to attain multiple substrate turnovers and high selectivity towards the Pt^{IV}-to-Pt^{II} conversion in a complex biological environment.

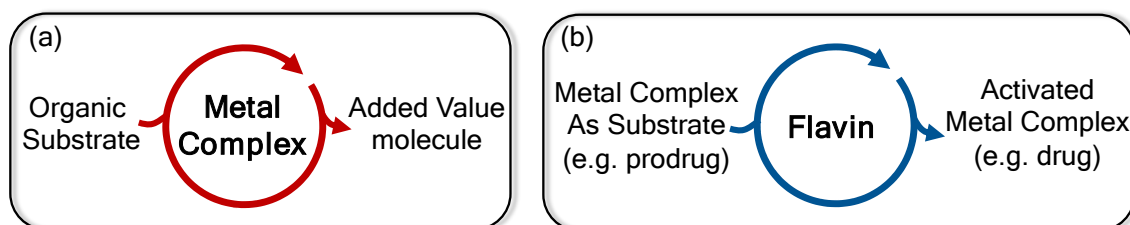


Figure 1. (a) Metal-based catalysis and (b) catalysis towards metal substrates.

Our proof-of-concept studies on flavins, Megger's enantioselective synthesis of [Ru(bpy)₃]²⁺ via organocatalysis⁷ and the recent aromatic amination of cyclometallated Ru^{II} and Rh^{III} octahedral complexes reported by Leonori⁸ are, to the best of our knowledge,

1
2 unique examples of catalytic reactions that use metal complexes as substrates. This
3 uncharted territory may offer intriguing opportunities to expand synthetic inorganic
4 chemistry and foster new catalysis-based applications for coordination and organometallic
5 compounds.
6
7
8

9 In view of such a perspective, this study aims at expanding the boundaries of catalysis
10 towards metal substrates by providing a detailed understanding of the mechanism through
11 which flavins (photo)catalyze the activation of Pt^{IV} complexes. Herein, we gather novel
12 insights into the catalytic mechanism and rationalize how changes in the structure of flavin
13 catalysts and Pt^{IV} substrates significantly affect reaction outcomes.
14
15
16

17 This work also reports fundamental information on the redox chemistry of flavins towards
18 transition metals. For instance, flavoenzymes such as mercuric reductase regulates Hg
19 resistance in several organisms by promoting the conversion of highly toxic Hg^{II} species
20 to less dangerous Hg⁰.⁹ Hence, findings described in this manuscript may have potential
21 implications in the biochemistry and in the cell homeostasis of metals.
22
23
24
25
26
27
28
29

30 RESULTS AND DISCUSSION

31 Catalysis studies

32 We employed five flavins and four Pt^{IV} prodrug complexes to investigate the catalyst and
33 substrate scope for the reduction of anticancer metal complexes (Figure 2). We selected
34 riboflavin (**Rf**), riboflavin-5'-phosphate (**FMN**), 2',3',4',5'-tetraacetylriboflavin (**TARF**) and
35 lumiflavin (**Lf**) to assess the role of the ribityl side chain in the catalytic transformation of
36 metal substrates. As shown in Figure S1 and in previous studies,¹⁰ the photostability of
37 flavin derivatives strongly depends on this fragment (**TARF** ~ **Lf** > **Rf** ~ **FMN**). The
38 flavoprotein **miniSOG** (mini Singlet Oxygen Generator)¹¹ was included in our panel of
39 catalysts to gauge the impact of an amino acid scaffold around the flavin catalytic core on
40 the catalysis. **MiniSOG** is a small FMN-containing fluorescent protein developed as CLEM
41 (correlative light and electron microscopy) tag¹¹ and investigated as photosensitizing
42 agent,^{12,13} including for photodynamic therapy.^{14,15} We opted for *cis,cis,trans*-
43 [Pt(NH₃)₂(Cl₂)(O₂CCH₂CH₂CO₂)₂]²⁻ (1), *cis,cis,trans*-
44 [Pt(NH₃)₂(O₄C₆H₆)(O₂CCH₂CH₂CO₂)₂]²⁻ (2), *cis,cis,trans*-[Pt(NH₃)₂(Cl₂)(O₂CCH₃)₂] (3),
45 *cis,cis,trans*-[Pt(NH₃)₂(O₄C₆H₆)(O₂CCH₃)₂] (4) as Pt^{IV} substrates because they are
46 structurally similar, and yet present features that could influence the catalytic process. We
47 envisaged that differences in the equatorial (chlorido *versus* cyclobutane dicarboxylato)
48 and axial (succinato *versus* acetato) ligands of the complexes could affect the catalysis.
49
50
51
52
53
54
55
56
57
58
59
60

Moreover, these complexes are of relevance in medicinal inorganic chemistry since they are either prodrugs of cisplatin (**1** and **3**) or carboplatin (**2** and **4**), two anticancer drugs clinically-approved worldwide.^{16,17}

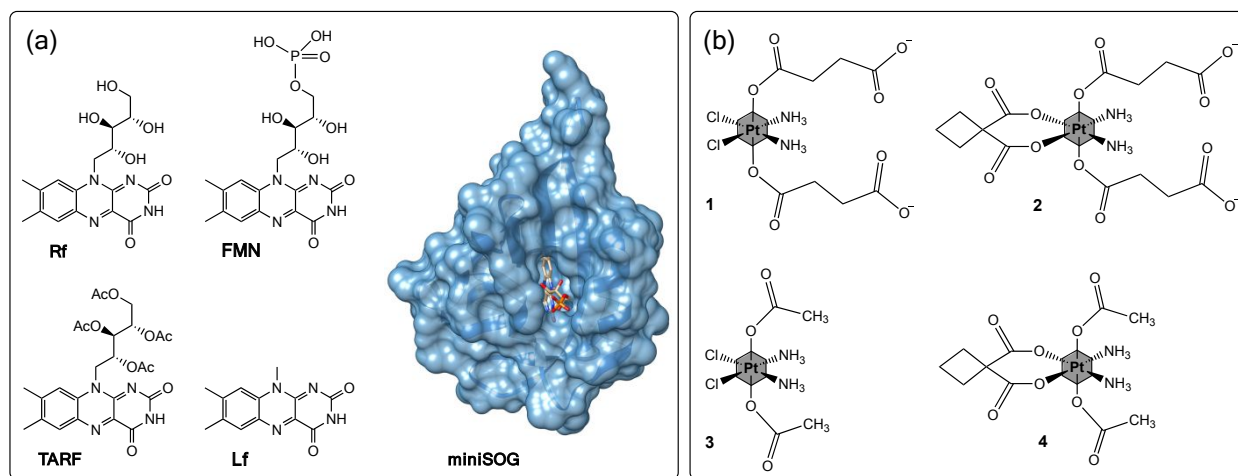


Figure 2. Structures of (a) catalysts and (b) substrates employed in this work. Catalysts: riboflavin (**Rf**), riboflavin-5'-phosphate (**FMN**), 2',3',4',5'-tetraacetylriboflavin (**TARF**), lumiflavin (**Lf**), mini Singlet Oxygen Generator (**miniSOG**). Substrates: *cis,cis,trans*-[Pt(NH₃)₂(Cl)₂(O₂CCH₂CH₂CO₂)₂]²⁻ (**1**), *cis,cis,trans*-[Pt(NH₃)₂(O₄C₆H₆)(O₂CCH₂CH₂CO₂)₂]²⁻ (**2**), *cis,cis,trans*-[Pt(NH₃)₂(Cl)₂(O₂CCH₃)₂] (**3**), *cis,cis,trans*-[Pt(NH₃)₂(O₄C₆H₆)(O₂CCH₃)₂] (**4**).

Unless otherwise stated, all photocatalysis experiments were performed in phosphate buffer (PB, 18 mM pH 7) using 25 μM catalyst (5% loading), 500 μM substrate (**1–4**) and 1 mM NADH (nicotinamide adenine dinucleotide) as electron donor. The choice of NADH was motivated by its participation in numerous biochemical redox reactions carried out by flavoproteins.¹⁸ Nevertheless, biological electron donors such as ascorbate can also be employed, whereas glutathione (GSH) is not efficacious in these reactions (**Figure S2 and S3**). Samples were irradiated with a 460-nm LED light source (6 mW·cm⁻²) in the presence of O₂. We evaluated reaction progression by ¹H NMR, monitoring the appearance and disappearance of diagnostic peaks corresponding to the coordinated and free succinato or acetato ligands of **1–4**. The release of such ligands corresponds to the formation of biologically active Pt^{II} species.²

The stability of complexes **1–4** (500 μM) was initially tested in PB (18 mM) with NADH (1 mM) over 48 h in the dark. We observed no decomposition of the Pt^{IV} substrates in the absence of FLs (**Figure S4**). When flavins (25 μM) were added to the PB buffered solution, conversion of **1–4** slowly occurred reaching 40 to 100 % after 16 h, except in the case of samples containing **miniSOG** that showed barely any change after 48 h (**Figure S5–S9**). Experiments performed using **Rf** and **1** (**Figure S10**) revealed that the dark conversion of

the substrate was faster at higher concentrations of **Rf** (50–150 μM) and NADH (2.5 and 5 mM).

Dark reactivity of the different catalysts towards the substrates did not follow any specific trend. Complexes **2** and **4** partially afforded (5–40%) free cyclobutane dicarboxylate (CBDA) ligand as reaction product in the presence of **FMN**, **TARF** and **Lf**. In addition, the photostability of metal substrates **1–4** was tested in the presence of 1 mM NADH (18 mM PB, pH 7) under 460-nm light irradiation. Complexes **1** and **3** underwent approximately 20% conversion over 3 h, while carboplatin derivatives did not show any light-induced reactivity (Figure S11). Under light irradiation, solutions containing **1–4** and catalytic amounts of **Rf** did not present any significant substrate conversion in the absence of NADH (Figure S12), confirming the need for an electron donor for the catalysis to occur.

Table 1 and Figure 3 summarize catalysis results obtained for the different flavin catalysts and metal substrates under the conditions described above (see also, Figure S13–17).

Table 1. Turnover frequencies (TOFs, min^{-1}), turnover numbers (TONs) and conversion (Conv.) percentages for the flavin-catalyzed photoactivation of **1–4** in the presence of NADH.

Complex	TOF (min^{-1})	TON	Conv. [%]
Rf			
1	17.3 \pm 0.6	20	100
2	8.1 \pm 0.4	20	100
3	20.3 \pm 2.0	20	100
4	10.0 \pm 0.3	20	100
FMN			
1	19.3 \pm 1.7	20	100
2	13.4 \pm 0.9	17.9 \pm 0.2	89.9 \pm 0.9
3	23.2 \pm 1.7	20	100
4	15.5 \pm 1.4	20	100
TARF			
1	24.1 \pm 5.1	20	100
2	13.7 \pm 0.2	18.5 \pm 0.2	92.4 \pm 1.0
3	26.0 \pm 1.1	20	100
4	22.7 \pm 5.6	20	100
Lf			
1	9.2 \pm 0.1	20	100
2	2.6 \pm 1.6	20	100
3	13.3 \pm 0.5	20	100
4	7.9 \pm 1.0	20	100
miniSOG			

1	3.7 ± 0.2	20	100
2	1.3 ± 0.3	14.7 ± 0.7	73.4 ± 3.8
3	5.6 ± 0.3	18.7 ± 1	93.7 ± 5.5
4	2.6 ± 0.4	17.5 ± 0.6	87.7 ± 3.1

Photocatalytic reactions reached full conversion of **1–4** and turnover numbers (TONs) of 20 upon few minutes of light irradiation, the only exception being **2** with **FMN** and **TARF** and **2–4** with **miniSOG**. TOF values for free **FMN** were 4–6 times higher compared to **FMN**-embedded in **miniSOG**, and in the case of **2** even up to 10-fold higher. Notably, TONs reached significantly higher values when lower catalyst loading (0.2%, 1 μM) and longer irradiation periods were employed. In the case of **Rf**, we observed TONs of 500 for **1** and **3** and of 423 and 468 for **2** and **4** respectively, upon approximately 2 h of light irradiation (Figure S18).

In general, cisplatin prodrugs **1** and **3** were more efficiently converted compared to their carboplatin analogues **2** and **4**, affording superior turnover frequency values (TOF, min⁻¹). The preference for cisplatin prodrugs was confirmed in substrate competitive experiments in which the conversion of couples of substrates was simultaneously tested (Figure S19 and S20).

Complex **3** showed the highest TOF for all flavin catalysts. The catalytic activity of **Lf** resulted in significantly lower TOFs compared to other flavins, reasonably suggesting that the ribityl chain plays an important role in the catalytic process (*vide infra*). Overall,

miniSOG resulted the least efficient catalyst, with TOF values ranging 1.3–5.6 min⁻¹, and showed similar reactivity as **Lf** towards substrate **2**. On average, the protein scaffold of **miniSOG** lowered reaction rates 6.4 times compared to free **FMN** which can be explained by the reduced substrate accessibility to the FMN when embedded in the protein.

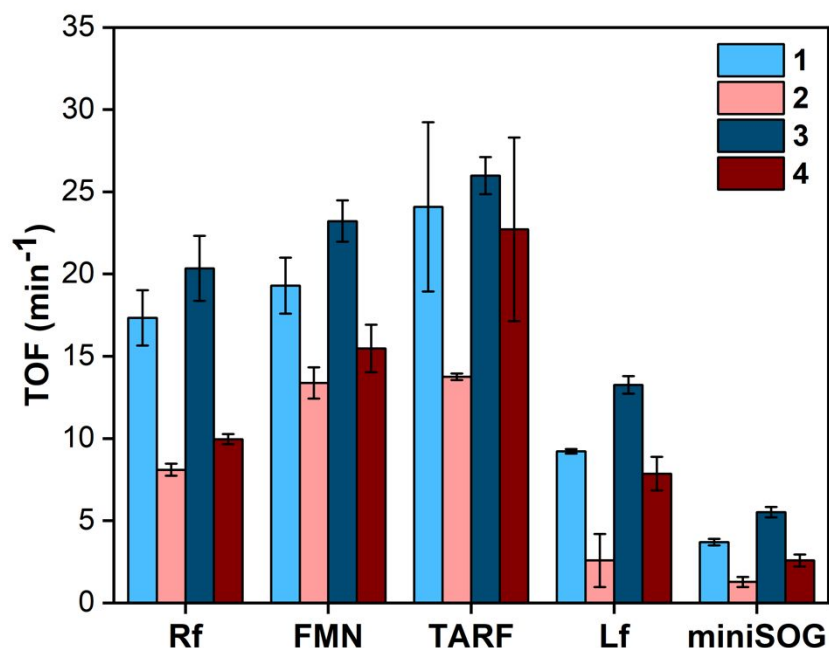


Figure 3. Turnover frequency values (TOF, min⁻¹) for the flavin-catalyzed photoactivation of 1–4.

Catalysis in cell culture medium

The application of catalysis towards metal substrates in the context of medicinal inorganic chemistry relies on the capability of flavins to convert the Pt^{IV} prodrugs in the biological environment, i.e. generate selectively Pt^{II} species in cells and/or their surroundings.^{2,3} Therefore, we studied how the flavin catalysts performed the activation of Pt^{IV} substrates in cell culture medium including fetal bovine serum (FBS). Such milieu contains a variety of chemicals and biological molecules that can interfere with the catalysis.

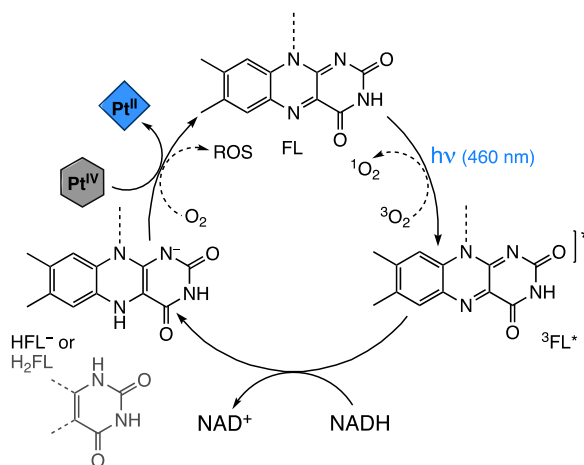
Substrates **1–4** were stable in medium containing 1 mM NADH for over 24 h in the dark (**Figure S21**). Upon addition of **Rf** (25 μM) the substrates were instead slowly transformed into their reaction products without the need for light excitation. Reactions were slow, and less than 40% conversion was observed in the first 8 h (**Figure S22**). The behavior of the other flavin catalysts was studied using **1** and **4**, because of their structural differences. In the dark, **FMN** and **Lf** performed similarly to **Rf**, promoting only partial substrate conversion at 8 h and full conversion at 24 h (**Figure S23 and S24**). **TARF** instead achieved full transformation of **1** and **4** within 1 h in the dark (**Figure S25**). Conversely, **miniSOG** did not show the capacity to carry out the activation of the substrates (24 h) in the absence of

1
2 light (Figure S26), which is a potential advantage for controlling the effects associated with
3 the activation of Pt^{IV} prodrugs in cells.
4

5 Under light irradiation, all FLs were dramatically efficient in converting **1** and **4**. For all
6 catalysts, the Pt^{IV} prodrugs were fully activated within 1 min, except in the case of **miniSOG**
7 which required more than 6–10 min (Figure S27 and S28). The quantification of reaction
8 efficiencies was problematic in cell culture medium due to the crowded spectrum and
9 signal overlapping. However, ¹H spectra evidenced that catalytic reactions were slightly
10 faster than in buffer solutions, suggesting that catalysts were not noticeably inactivated in
11 a more stringent biological environment and that they still recognized Pt^{IV} substrates
12 despite the presence of numerous other chemical and biological reactants. Therefore,
13 these results highlighted the bioorthogonal selectivity of flavin-mediated catalysis towards
14 Pt substrates and indicated that other electron donors present in the medium likely
15 contributed to the catalysis as well.
16
17
18
19
20
21
22
23
24
25

26 **Catalytic mechanism**

27 A plausible assumption for the mechanism of the Pt^{IV}-to-Pt^{II} photocatalytic conversion of
28 **1–4** implicates the formation of the triplet excited state (³FL*) of the flavin photocatalyst
29 through intersystem crossing after exciting its singlet state. ³FL* is a strong oxidant
30 capable of extracting 2 electrons from donors, such as NADH, to afford H₂FL or HFL⁻
31 depending on the pH of the solution.¹⁸ Such reduced flavin forms are the active catalytic
32 species that prompt the effective and bioorthogonal transformation of **1–4** (Scheme 1). In
33 the absence of light, the formation of H₂FL/HFL⁻ still takes place but is significantly less
34 efficient. Indeed, comparative experiments under O₂-free conditions showed that the
35 consumption of NADH by **FMN** is much slower in the dark than under irradiation (Figure
36 S29–S31). Furthermore, reduced flavins are readily oxidized by O₂ under aerobic
37 conditions to ultimately give H₂O₂.¹⁹ Thus, the conversion of Pt^{IV} substrates is much slower
38 in the absence of light, being H₂FL/HFL⁻ present at lower concentrations.
39
40
41
42
43
44
45
46
47
48
49
50
51
52
53
54
55
56
57
58
59
60



Scheme 1. Proposed mechanism for the catalytic conversion of substrates **1–4** by flavin catalysts.

To validate this mechanistic hypothesis, we studied in detail the reactivity of H₂FL/HFL⁻ towards **1** under oxygen-free conditions. N₂-purged solution of FMN and NADH (1:1, 15 μM in PB, pH 7.4) were irradiated at 460 nm for few seconds to obtain HFMN⁻ as confirmed by the appearance of its characteristic absorption spectrum and the concomitant disappearance of FMN bands at 400–500 nm (Figure 4a).²⁰ At pH above 7.0, HFL⁻ is the most abundant species for the catalysts tested in this work.¹⁸ Nevertheless, experiments at different pH, run using **1** and **3** and FMN indicated that both H₂FL and HFL⁻ could perform the catalysis with similar efficiency (Figure S14 and S32).

Of note, work by Hollmann^{21,22} demonstrated that light irradiation of flavin catalysts could boost reaction rates for the aerobic oxidation of reduced nicotinamide cofactors. Correspondingly, our results showed that use of NADH and visible light was effective in generating doubly reduced free flavins in oxygen free atmosphere. Compared to other established procedures,²³ this approach is advantageous since it avoids the use of high concentrations of strong reductants (e.g. sodium dithionite or borohydride) or the need of long photoreduction reactions with oxalate and UV light.

We obtained proof that HFMN⁻ is the catalytic active species by monitoring the evolution of its UV-Vis spectrum upon addition of **1** (54 μM, final concentration) under anaerobic conditions. As shown in Figure 4a, HFMN⁻ was promptly re-oxidized and the absorption features of FMN restored once the Pt^{IV} substrate was added. Under similar conditions (i.e. no O₂, 3.3 mM FMN and NADH, PB, pH 7.4), ¹H NMR resonances of FMN disappeared in the presence of NADH upon light irradiation (Figure 4b), consistently with the conversion to HFMN⁻, and reemerged only after successive additions of **1** (4 mM, final concentration). The presence of the singlet signal correspondent to free succinate confirmed the

conversion of the Pt^{IV} substrate. Once an excess of substrate was added (Figure 4b), signals relative to unreacted **1** became clearly visible again. As previously reported by Gschwind and coworkers,^{24,25} line broadening due to proton exchange prevented direct detection of ¹H NMR signals relative to reduced flavin species in aqueous solutions. Equivalent results were obtained by UV-Vis for **TARF** and **Lf** using **1** as substrate (Figure S33 and S34).

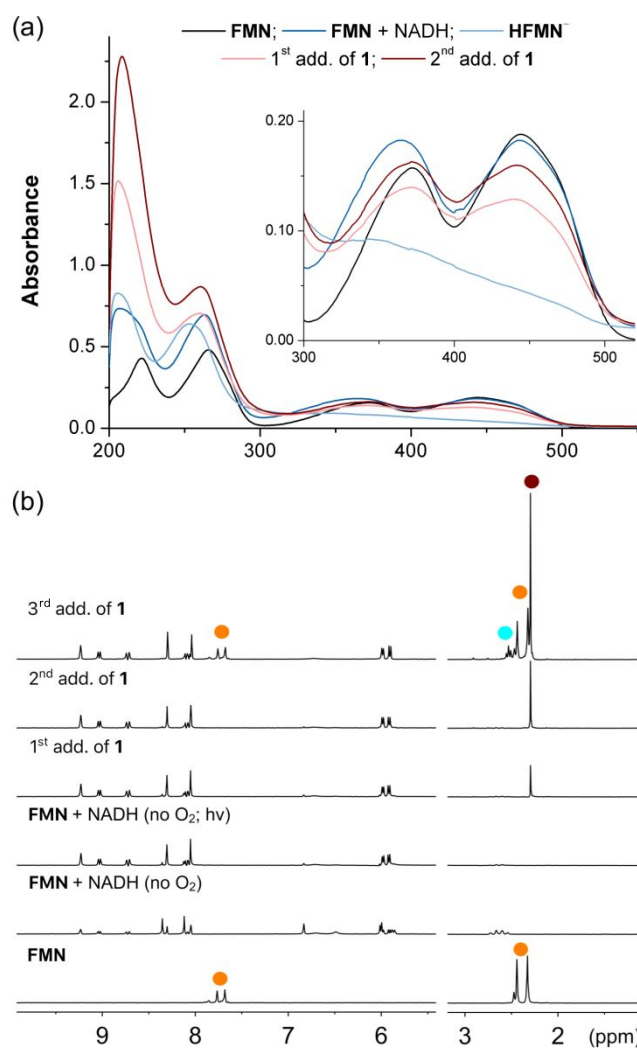
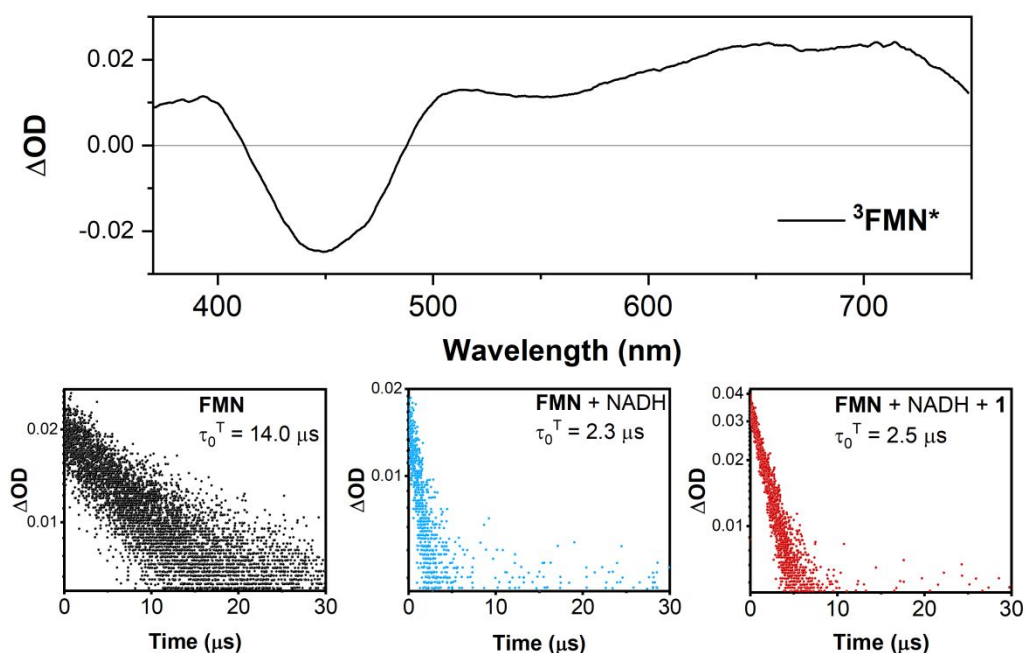


Figure 4. (a) UV-Vis and (b) NMR characterization of the key catalytic species **HFMN⁻** and its reactivity towards **1**. **HFMN⁻** (a: 15 μ M; b: 3.3 mM) generated using 1 mol equiv. of NADH upon 460-nm light irradiation (6 mW \cdot cm⁻², a: 40 s; b: 360 s) in the absence of O₂ (18 mM PB, pH 7.4). Final concentrations of **1** were 54 μ M and 4 mM for UV-Vis and NMR experiments, respectively. ¹H NMR signal labelling: ● **FMN**; ● free -O₂CCH₂CH₂CO₂⁻; ● **1** (Pt-OCOCH₂CH₂CO₂⁻).

Time-resolved optical spectroscopy proved that generation of HFL⁻ occurred via initial reductive quenching of the ³FL* excited state by NADH. In first instance, fluorescence emission lifetime measurements performed on **FMN** ($\lambda_{\text{exc}} = 445$ nm, $\lambda_{\text{em}} = 540$ nm, Figure S35) indicated that its singlet excited state decay ($\tau_{\text{Fluo}} = 4.7$ ns) was not altered by the

presence of NADH (1:20) or NADH and **1** (1:20:20), therefore ruling out the involvement of such state in the catalytic process. However, the case for the $^3\text{FMN}^*$ excited state was different, as demonstrated by flash photolysis experiments (Figure 5, Figure S36). Previous work²⁶ showed that the evolution of the triplet state of **Rf** in the presence of quenchers can be monitored by the decay of its characteristic triplet-triplet absorption band. For this reason, we measured the transient absorption spectrum of **FMN** ($\lambda_{\text{exc}} = 445$ nm) in a de-aerated solution and determined the triplet lifetime in the presence of NADH and **1**. Consistently with the literature, $^3\text{FMN}^*$ displayed an intense and negative contribution in the 420–480 nm range, corresponding to the ground state bleaching associated with the $S_0 \rightarrow S_1$ transition. The positive band at around 600–720 nm was attributed to the absorption of the T_1 state. The assignment of the triplet-state absorption was also confirmed by its quenching in the presence of O_2 . The **FMN** triplet lifetime in a de-aerated solution (τ_0^T) was 14 μs (Figure 5) long enough for an efficient quenching by O_2 , which indeed reduced τ^T to 4 μs in air-saturated samples (Figure S36). In the presence of an NADH excess (1:20), we observed that τ_0^T decreased as well, from 14 μs to 2.3 μs , confirming the reductive quenching of $^3\text{FMN}^*$ by this electron donor. Nevertheless, no further significant changes were observed on τ_0^T once **1** (1:20:20) was added to the solution containing both **FMN** and NADH. This result indicated that the Pt^{IV} conversion process does not involve $^3\text{FMN}^*$, but rather the ground-state HFMN^- species in agreement with UV-Vis and NMR data (Figure 4). Similar findings were obtained tracking the triplet excited state decay in air saturated solutions (Figure S36).



1
2 **Figure 5.** Transient absorption spectrum (λ_{exc} 445 nm) of $^3\text{FMN}^*$ and decays (τ_0^T) of the triplet-triplet
3 absorption at 700 nm for N_2 -deaerated solutions of **FMN** (20 μM), **FMN** (20 μM) + NADH (400 μM), and **FMN**
4 (20 μM) + NADH (400 μM) + **1** (400 μM).
5
6
7

8 Considering that reduction potentials for **1–4** are more negative (**Figure S37**) than FLs, an
9 outer sphere reduction of the substrates would be a neat uphill reaction. For this reason,
10 formation of substrate- $\text{H}_2\text{FL}/\text{HFL}^-$ intermediates, and possibly a ligand-bridged inner
11 sphere mechanism, might promote the flavin-mediated reduction of Pt^{IV} complexes.²⁷
12 These adducts could trigger the conversion of **1–4** in to their Pt^{II} counterparts at a less
13 negative potential.¹² Furthermore, specific catalyst-substrate interactions could also
14 explain the bioorthogonal selectivity of these reactions.
15

16 Density functional theory (DFT) calculations indicated that such a scenario is reasonable.
17 Indeed, we optimized a number of substrate- $\text{H}_2\text{Rf}/\text{HRf}^-$ adducts stabilized by hydrogen
18 bonding interactions between the ligands of the Pt complexes and the isoalloxazine and
19 ribityl moieties of FLs (**Figure 6**, **Figure S38** and **S39**). Consistently with the occurrence of
20 reduction and ligand elimination reactions, optimized geometries displayed electronic
21 structures in which the HOMO (highest occupied molecular orbital) is centered on
22 $\text{H}_2\text{Rf}/\text{HRf}^-$, while the LUMO (lowest unoccupied molecular orbital) and LUMO+1 are σ -
23 antibonding orbitals localized on **1–4** (**Figure S40–42**). All optimized structures showed
24 interactions of the Pt-bound ligands with the ribityl chain, confirming that lack of this
25 fragment was consistent with a decrease in catalytic activity as observed for **Lf** towards all
26 substrates (**Table 1** and **Figure 3**). Furthermore, DFT highlighted that H-bonding between
27 **TARF** and the substrates were still possible, despite the acetylated ribityl chain of this
28 catalyst. In particular, we could optimize adduct geometries in which the NH_3 ligand of **1–**
29 **4** formed H-bonds with the $\text{C}=\text{O}(2'\text{C})$ of the ribityl and/or the N(5) of the isoalloxazine unit
30 of **TARF** (**Figure S43**).
31
32

33 The overall lower conversion efficiency for the carboplatin derivatives **2** and **4** compared
34 to their cisplatin counterparts **1** and **3** could instead be ascribed to the intrinsic
35 thermodynamic stability of the Pt complexes. In fact, the corresponding axial and
36 equatorial ligand exchange energy, calculated with different DFT functionals (**Figure S44**),
37 indicated that **1** and **3** are less stable than **2** and **4**, respectively. The same holds true for
38 succinato versus acetato ligands, having **3** lower stability than **1** and **4** than **2**. These trends
39 are also in good agreement with reduction potentials of the complexes (**Figure S37**).
40
41
42
43
44
45
46
47
48
49
50
51
52
53
54
55
56
57
58
59
60

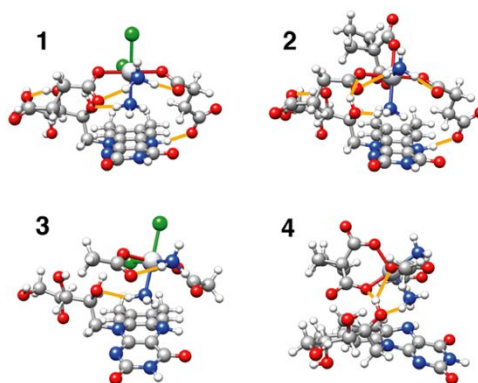


Figure 6. DFT-optimized (pbe0/def2-SVP) structures of adducts between **1–4** and RfH^- (H-bond contacts highlighted with orange lines).

In order to further rationalize the lower stability of cisplatin derivatives with respect to carboplatin ones, we also analyzed the DFT atomic charge of the Pt atom in **1–4** and their corresponding Pt^{II} drugs. Irrespective of the functional or the atomic charge evaluation method used, the Pt atom showed a significant lower positive charge in cisplatin than in carboplatin, as well as in their corresponding Pt^{IV} prodrugs (Figure S37). Therefore, the electrostatic interaction between the Pt center and its equatorial ligands is weaker in the case of cisplatin derivatives compared to carboplatin complexes, and consequently **1** and **3** are more easily converted than **2** and **4**. On the other hand, since succinato ligands bear a doubly negative charge at neutral pH ($\text{pK}_{\text{a}1} = 4.2$ and $\text{pK}_{\text{a}2} = 5.6$), whereas acetato ligands ($\text{pK}_{\text{a}} = 5.5$) are only singly negatively charged, the Pt-acetato bond is weaker than the Pt-succinato one, and therefore easier to activate. These stability trends for **1–4** can be traced back to the stabilization of the Pt-ligand bonds, and provide an overall good explanation for the different prodrug conversion efficiencies found in this work.

MiniSOG has an FMN embedded in the protein structure and showed a more intricate photochemistry. Upon light irradiation and in the absence of electron donors and O_2 , **miniSOG** generated the $\text{FMN}^{\cdot-}$ radical (semiquinone) that displayed a broad absorption peak at ca. 600 nm (Figure S46). This process was previously ascribed to the oxidation of certain amino acids and is known to compete with the capacity of **miniSOG** to generate $^1\text{O}_2$ with high yields.^{28–30} Upon exposing irradiated solutions of **miniSOG** to the oxygen-containing ambient atmosphere, the spectral features of $\text{FMN}^{\cdot-}$ disappeared and the absorbance at 450 nm was almost completely recovered (Figure S46). Conversely, **1** poorly reacted with the radical when incubated with **miniSOG**. This effect was observed by UV-Vis and ^1H NMR experiments (Figure S47 and S48), in which stoichiometric quantities

of light-irradiated **miniSOG** in the absence of O₂ could transform **1** much slower than under the standard aerobic catalysis conditions.

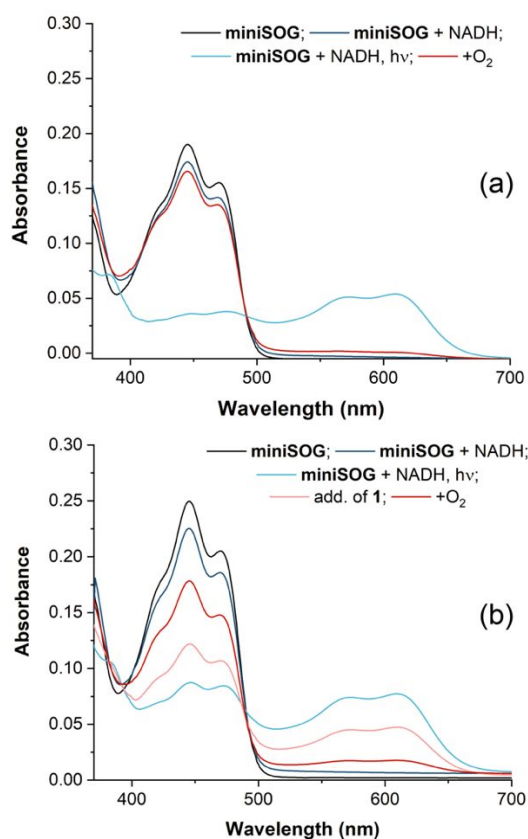


Figure 7. UV-Vis monitoring of light-irradiated **miniSOG** under anaerobic conditions upon addition of electron acceptors: (a) O₂ and (b) **1** (120 μM). Solutions of **miniSOG** (15 μM, 18 mM PB, pH 7.4) were irradiated (6 mW·cm⁻², 180 s) in the presence of 1 mol equiv. of NADH and in the absence of O₂.

In the presence of NADH, electron transfer from the protein scaffold was not shut down and the FMN^{•-} radical could still be detected (Figure 7a and b). Nevertheless, UV-Vis spectra revealed that doubly-reduced FMN was also obtained, as indicated by the marked absorbance decrease at 400–500 nm. Exposure of such solution to either O₂ or **1** (120 μM) caused the regeneration of FMN indicating that HFMN^{•-} was likely the major active catalytic species towards the Pt substrates for **miniSOG** as well. So, quenching of FMN excited state by photooxidation of amino acid residues competed with the formation of the active catalysts, in a similar fashion to what has been observed for ¹O₂ sensitization. Compared to other FLs tested herein, the lower conversions and TOF values of **miniSOG** should also be ascribed to the reduced substrate accessibility of its FMN.

As shown here for **miniSOG** and for other FL catalysts in Figure S49, O₂ functioned as electron sink to deactivate doubly and singly-reduced FLs. This behavior is not surprising considering the biochemistry of flavins and flavoproteins. However, it suggests that the

1
2 role of O₂ in the catalytic conversion of **1–4** ought to be evaluated for a thorough
3 comprehension of the catalytic mechanism. In addition, FLs such as the one tested in this
4 work are well known singlet-oxygen (¹O₂) photosensitizers.^{13,31}

5
6
7 Monitoring the photoactivation kinetics of **1–4** in aerated solutions, we observed an
8 induction period for all FL catalysts (Figure S50) at short light irradiation times. This finding
9 is consistent with the presence of competitive catalytic cycles that involve the
10 transformation of O₂ in ¹O₂ and reactive oxygen species (ROS). Under anaerobic
11 conditions, conversion of substrates readily occurs. Conversely, as shown for **1** and **FMN**
12 (Figure S51), the reaction does not reach completion and kinetics is significantly slower
13 when air is bubbled into the solution.

14
15
16 FL catalysts can interact with O₂ in the ³FL* excited state to give ¹O₂ or once reduced to
17 HFL⁻ to generate ROS such as O₂^{•-} and H₂O₂ (Scheme 1). We confirmed the occurrence
18 of both pathways by means of indirect optical methods previously validated for **FMN** and
19 **miniSOG**.^{12,29} That is, we employed uric acid and hydroethidine as molecular probes for
20 the formation of ¹O₂ and ROS, respectively. We observed that **FMN** and **miniSOG** solutions
21 irradiated in the presence of an excess of NADH and **1** showed indeed production of both
22 (Figure S52–S54). As described previously,^{12,29} free **FMN** is a better ¹O₂ photosensitizer
23 than **FMN** embedded in the **miniSOG** scaffold, in agreement with the self-quenching of its
24 triplet excited state by the protein matrix in the latter case. However, **miniSOG** generation
25 of ROS was almost comparable to **FMN**, reasonably because O₂^{•-} is readily formed by
26 photoinitiated electron-transfer reactions involving the protein (e.g. from FMN⁻). Control
27 experiments run in the absence of NADH and **1** did not show a significant decrease in the
28 generation of ¹O₂ and ROS, suggesting that O₂ was immediately converted by flavins in
29 such photoproducts, before the catalysis towards Pt substrates took place.

30 31 32 33 34 35 36 37 38 39 40 41 42 43 44 45 46 47 **CONCLUSIONS**

48 This work expands the scope of flavin-mediated photocatalysis towards platinum
49 substrates, providing new fundamental mechanistic details. The reduced H₂FL/HFL⁻
50 species has been identified by optical spectroscopy and NMR under anaerobic conditions
51 as the active catalyst. H-bond interactions between H₂FL/HFL⁻ and the Pt^{IV} substrates
52 may be crucial in promoting the conversion to Pt^{II} drugs, possibly via a ligand-bridged
53 inner sphere reduction mechanism. The ribityl chain could stabilize these putative
54 intermediates and increase the catalytic efficiency of the reactions. For this reason, **Lf**
55 showed the lowest TOFs among the free FLs tested. Self-quenching of the **miniSOG**
56
57
58
59
60

excited states by protein amino acids reduced the efficiency of this catalyst, as similarly observed for its $^1\text{O}_2$ photosensitization capacity. Structural modifications of the ribityl group in free FLs and site mutagenesis in **miniSOG** are worth investigating in the future to boost their catalytic activity and widen the repertoire of this new chemistry towards different metals.

EXPERIMENTAL SECTION

Materials

Riboflavin (**Rf**), riboflavin 5'-monophosphate sodium salt hydrate (**FMN**), potassium phosphate monobasic, potassium phosphate dibasic, β -nicotinamide adenine dinucleotide, reduced disodium salt hydrate, sodium dithionite, RPMI-1640 medium were purchased from Sigma-Aldrich, potassium tetrachloroplatinate(II) from Precious Metals Online. All chemicals were used as received without additional purification. The fetal bovine serum (10%) added to the RPMI-1640 medium was purchased from Invitrogen.

Preparation of substrates and catalysts. Complexes *cis,cis,trans*-[Pt(NH₃)₂(Cl₂)(O₂CCH₂CH₂CO₂)₂]²⁻ (**1**), *cis,cis,trans*-[Pt(NH₃)₂(O₄C₆H₆)(O₂CCH₂CH₂CO₂)₂]²⁻ (**2**), *cis,cis,trans*-[Pt(NH₃)₂(Cl₂)(O₂CCH₃)₂] (**3**), *cis,cis,trans*-[Pt(NH₃)₂(O₄C₆H₆)(O₂CCH₃)₂] (**4**) were synthesized and characterized as previously reported.³²⁻³⁴ Tetra-O-acetyl riboflavin (**TARF**) and lumiflavin (**Lf**) were prepared following the procedure reported by I. Jhulki *et al.*³⁵ **MiniSOG** was prepared and purified as previously reported by us.³

Methods

Nuclear magnetic Resonance (NMR). ¹H NMR spectra of the various samples were recorded on a Fourier TM Bruker 300 NMR and on an AVANCE III Bruker 500 NMR spectrometer using standard pulse programs. Chemical shifts were reported in parts-per-million (δ , ppm) and referenced to the residual solvent peak.

Catalysis experiments. Unless otherwise specified, all reactions were carried out in air at 298 K and pH 7.0 using 25 μM catalyst, 500 μM substrate (**1-4**) and 1 mM NADH. Light irradiation experiments were performed employing an LED light source ($\lambda_{\text{max}} = 460 \text{ nm}$, 6 $\text{mW}\cdot\text{cm}^{-2}$).⁴ Turnover frequency (TOF), turnover number (TON) and % conversion for the catalytic reactions were determined by quantifying the amount of converted **1-4** via ¹H

1
2 NMR. Integration of the free succinato and acetato ligand signals (singlets at 2.25–2.35
3 ppm and at approx. 1.80 ppm respectively) were used for monitoring the reaction
4 progress. TOF values were obtained at substrate conversions of 25–35%.
5
6
7

8
9 **UV-Vis absorption spectroscopy (UV-Vis).** All spectra were acquired in optical quartz
10 cuvettes in aqueous solutions or buffers using a JASCO V-730 spectrophotometer.
11
12

13
14 **Fluorescence emission and lifetimes.** The emission spectrum of **FMN** (20 μM) was recorded
15 on a spectrofluorimeter Edinburgh Instruments (FL920 model) with a 450 W xenon flash
16 lamp as the excitation source. Fluorescence radiative decay curves were recorded with a
17 time-correlated single-photon counting technique (Edinburgh Instruments, model FL920)
18 at $\lambda_{\text{em}} = 540$ nm after excitation at $\lambda_{\text{exc}} = 445$ nm by means of a fianium supercontinuous
19 wavelength tunable-laser with 150 ps FWHM pulses using a microchannel plate detector
20 (Hamamatsu C4878) with picosecond time resolution. Fluorescence lifetimes were
21 obtained after deconvolution of the instrumental response signal from the recorded decay
22 curves by means of an iterative method. The goodness of the exponential fit was
23 controlled by statistical parameters (χ^2 and analysis of the residuals). Measurements were
24 performed on air-saturated solutions of (a) **FMN** (20 μM), (b) **FMN** (20 μM) and NADH (400
25 μM), and (c) **FMN** (20 μM), NADH (400 μM) and **1** (400 μM).
26
27
28
29
30
31
32
33
34
35

36
37 **Transient absorption and triplet lifetimes.** Nanosecond transient absorption measurements
38 were recorded on a LP980 laser flash photolysis spectrometer (Edinburgh Instruments,
39 Livingston, UK). Samples were excited by a nanosecond pulsed laser (Nd:YAG
40 laser/OPO, LOTIS TII 2134) at the absorption maxima (445 nm) operating at 1 Hz and
41 with a pulse width of 7 ns at a 10 mJ excitation power. Samples with an optical absorbance
42 of 0.3 at the excitation wavelength were either deaerated with nitrogen for ca. 10 min or
43 aerated for ca. 10 min with air. Transient spectra were recorded on ICCD detector
44 (DH320T TE cooled, Andor Technology). The decay of triplet-triplet absorption in the
45 presence and absence of oxygen (nitrogen and air saturated solutions) were collected at
46 700 nm on single detector (PMT R928P) and oscilloscope. Triplet lifetimes in absence
47 and presence of oxygen (τ_0^T and τ^T) were obtained from the slope of the recorded decay
48 curves by means of an iterative method by LP900 software. The goodness of the
49 exponential fit was controlled by statistical parameters (χ^2). Solutions of (a) **FMN** (20 μM),
50
51
52
53
54
55
56
57
58
59
60

1
2 (b) **FMN** (20 μM) and **NADH** (400 μM), and (c) **FMN** (20 μM), **NADH** (400 μM) and **1** (400
3 μM) were employed for in this set of experiments.
4
5

6
7 **Singlet oxygen and ROS production.** Quantification of $^1\text{O}_2$ and ROS was achieved using
8 methods previously established for **FMN** and **miniSOG**.^{12,29} Indirect measurement of $^1\text{O}_2$
9 was performed using uric acid (UA) as probe³⁶ and monitoring the changes of its
10 absorbance at 292 nm over light irradiation time. We exposed to 460-nm light (6 $\text{mW}\cdot\text{cm}^{-2}$)
11 optically-matched solutions containing UA (50 μM) and (a) **FMN/miniSOG** (5 μM), (b)
12 **FMN/miniSOG** (5 μM) and **NADH** (30 μM), and (c) **FMN/miniSOG** (5 μM), **NADH** (30 μM)
13 and **1** (15 μM).
14
15

16
17 Photooxidation of hydroethidine (HE) was instead used to evaluate the production of other
18 ROS (particularly $\text{O}_2^{\cdot-}$) since the transformation of this probe does not occur upon
19 interaction with $^1\text{O}_2$.^{29,37} Also in this case, HE (50 μM) solutions containing (a)
20 **FMN/miniSOG** (5 μM), (b) **FMN/miniSOG** (5 μM) and **NADH** (30 μM), and (c) **FMN/miniSOG**
21 (5 μM), **NADH** (30 μM) and **1** (15 μM) were irradiated at 460 nm and their fluorescence
22 intensity collected at different time points ($\lambda_{\text{ex}} = 525 \text{ nm}$, $\lambda_{\text{em}} = 550\text{--}800 \text{ nm}$) as described
23 previously.²⁹
24
25
26
27
28
29
30
31

32
33 **Electrochemistry.** Cyclic voltammetry experiments were performed using a Metrohm
34 Autolab 302N potentiostat. The electrochemical cell was a single-compartment cell
35 equipped with a standard three-electrode set-up: a glassy carbon working electrode ($\varnothing =$
36 1 mm), a Pt-wire counter electrode and a saturated calomel electrode (SCE) as
37 reference. All measurements were carried out in deoxygenated condition under argon
38 atmosphere, employing a 0.05 M phosphate buffer (pH 7.4) containing 0.15 M NaCl.
39 Solutions for metal complexes were $5.0\cdot 10^{-4}$ M. **FMN** and **Rf** were measured at $2.7\cdot 10^{-4}$
40 and $2.0\cdot 10^{-4}$ M respectively, while **TARF** and **Lf** voltammogram were obtained using
41 saturated solutions due to poor solubility. The working electrode was polished with
42 alumina, rinsed with distilled water and dried before each potential sweep to ensure
43 reproducible surface for all experiments.
44
45
46
47
48
49
50
51
52

53
54 **Computational methods.** All calculations were performed with Gaussian 16, Revision
55 B01.³⁸ Geometry optimizations of substrate-riboflavin adducts were run at the DFT level
56 using the pbe0/def2-SVP combination.^{39,40} Solvent was introduced by means of the
57 polarized continuum model (PCM) with water as implicit solvent, and dispersion
58
59
60

1
2 interactions were taken into account using Grimme's dispersion correction with Becke and
3 Johnson's damping.⁴¹ The frequencies were then used to evaluate the zero-point
4 vibrational energy (ZPVE) and the thermal (T = 298 K) vibrational corrections to the
5 enthalpies and Gibbs free energies within the harmonic oscillator approximation. To
6 calculate the entropy, the different contributions to the partition function were evaluated
7 using the standard statistical mechanics expressions in the canonical ensemble and the
8 harmonic oscillator and rigid rotor approximation. Energy calculations for the relative
9 stability of substrates 1–4 were performed using the def2-TVP basis set⁴⁰ and three
10 different functionals, namely pbe0, wb97xd⁴² and m062x.⁴³ We calculated atomic charges
11 using the same combination of functionals and basis set together with the nbo⁴⁴ and
12 chelpg⁴⁵ methods.

23 24 **AUTHOR INFORMATION**

25 **Corresponding Author**

26 E-mail*: lsalassa@dipc.org

29 30 **ORCID**

31 Virginia Martínez-Martínez: 0000-0001-7551-3714

32 Claudio Garino: 0000-0002-7854-6076

33 Fabrizio Mancin: 0000-0003-0786-0364

34 Aitziber L. Cortajarena: 0000-0002-5331-114X

35 Luca Salassa: 0000-0002-2112-9095

38 39 40 41 **Notes**

42 The authors declare no competing financial interest.

43 44 45 46 **ASSOCIATED CONTENT**

47 The Supporting Information is available free of charge on the ACS Publications website
48 at DOI:XXXX.

49 Stability and catalysis experiments (NMR and UV-Vis), electrochemistry, time-resolved
50 spectroscopy data and DFT results.

51 52 53 54 55 **ACKNOWLEDGMENTS**

56 We acknowledge financial support from the Spanish MINECO (grant CTQ2016-80844-R,
57 BIO2016-77367-R, PCI2018-092984 and MAT2017-83856-C3-3-P), Eusko Jauriaritza

(Elkartek KK-2017/00008, IT588-13 and IT912-16), UPV/EHU (PES14/35), and the European Research Council (ERC-CoG-648071). This work was performed under the Maria de Maeztu Units of Excellence Program from the Spanish State Research Agency – Grant No. MDM-2017-0720 (CIC biomaGUNE). We thank Dr. Á. Martínez for support in the synthesis of TARF and Lf. Authors acknowledge the technical and human support provided by the IZO-SGI SGIker of UPV/EHU.

REFERENCES

- (1) Alonso-de Castro, S.; Terenzi, A.; Gurruchaga-Pereda, J.; Salassa, L. Catalysis Concepts in Medicinal Inorganic Chemistry. *Chem. – A Eur. J.* **2019**, *25*, 6651–6660. <https://doi.org/10.1002/chem.201806341>.
- (2) Alonso-de Castro, S.; Terenzi, A.; Hager, S.; Englinger, B.; Faraone, A.; Martínez, J. C.; Galanski, M.; Keppler, B. K.; Berger, W.; Salassa, L. Biological Activity of Pt^{IV} Prodrugs Triggered by Riboflavin-Mediated Bioorthogonal Photocatalysis. *Sci. Rep.* **2018**, *8*, 17198. <https://doi.org/10.1038/s41598-018-35655-2>.
- (3) Alonso-de Castro, S.; Cortajarena, A. L.; López-Gallego, F.; Salassa, L. Bioorthogonal Catalytic Activation of Platinum and Ruthenium Anticancer Complexes by FAD and Flavoproteins. *Angew. Chemie Int. Ed.* **2018**, *57*, 3143–3147. <https://doi.org/10.1002/anie.201800288>.
- (4) Alonso-de Castro, S.; Ruggiero, E.; Ruiz-de-Angulo, A.; Rezabal, E.; Mareque-Rivas, J. C.; Lopez, X.; López-Gallego, F.; Salassa, L. Riboflavin as a Bioorthogonal Photocatalyst for the Activation of a Pt^{IV} Prodrug. *Chem. Sci.* **2017**, *8*, 4619–4625. <https://doi.org/10.1039/C7SC01109A>.
- (5) Ngo, A. H.; Bose, S.; Do, L. H. Intracellular Chemistry: Integrating Molecular Inorganic Catalysts with Living Systems. *Chem. – A Eur. J.* **2018**, *24*, 10584–10594. <https://doi.org/10.1002/chem.201800504>.
- (6) Martínez-Calvo, M.; Mascareñas, J. L. Organometallic Catalysis in Biological Media and Living Settings. *Coord. Chem. Rev.* **2018**, *359*, 57–79. <https://doi.org/10.1016/j.ccr.2018.01.011>.
- (7) Gong, L.; Lin, Z.; Harms, K.; Meggers, E. Isomerization-Induced Asymmetric Coordination Chemistry : From Auxiliary Control to Asymmetric Catalysis**. *Angew. Chemie - Int. Ed.* **2010**, No. 49, 7955–7957. <https://doi.org/10.1002/anie.201003139>.
- (8) Ruffoni, A.; Juliá, F.; Svejstrup, T. D.; McMillan, A. J.; Douglas, J. J.; Leonori, D.

- 1
2 Practical and Regioselective Amination of Arenes Using Alkyl Amines. *Nat. Chem.*
3 **2019**, *11*, 426–433. <https://doi.org/10.1038/s41557-019-0254-5>.
- 4
5
6 (9) Barkay, T.; Miller, S. M.; Summers, A. O. Bacterial Mercury Resistance from Atoms
7 to Ecosystems. *FEMS Microbiol. Rev.* **2003**, *27*, 355–384.
8 [https://doi.org/10.1016/S0168-6445\(03\)00046-9](https://doi.org/10.1016/S0168-6445(03)00046-9).
- 9
10
11 (10) Edwards, A. M.; Bueno, C.; Saldaño, A.; Silva, E.; Kassab, K.; Polo, L.; Jori, G.
12 Photochemical and Pharmacokinetic Properties of Selected Flavins. *J. Photochem.*
13 *Photobiol. B Biol.* **1999**, *48*, 36–41. [https://doi.org/10.1016/S1011-1344\(99\)00006-](https://doi.org/10.1016/S1011-1344(99)00006-8)
14 [8](https://doi.org/10.1016/S1011-1344(99)00006-8).
- 15
16
17
18 (11) Shu, X.; Lev-Ram, V.; Deerinck, T. J.; Qi, Y.; Ramko, E. B.; Davidson, M. W.; Jin,
19 Y.; Ellisman, M. H.; Tsien, R. Y. A Genetically Encoded Tag for Correlated Light and
20 Electron Microscopy of Intact Cells, Tissues, and Organisms. *PLOS Biol.* **2011**, *9*,
21 e1001041.
22
- 23
24
25 (12) Agut, M.; Ruiz-González, R.; Cortajarena, A. L.; Flors, C.; Mejias, S. H.; Nonell, S.
26 Singlet Oxygen Generation by the Genetically Encoded Tag MiniSOG. *J. Am.*
27 *Chem. Soc.* **2013**, *135*, 9564–9567. <https://doi.org/10.1021/ja4020524>.
- 28
29
30 (13) Rodríguez-Pulido, A.; Cortajarena, A. L.; Torra, J.; Ruiz-González, R.; Nonell, S.;
31 Flors, C. Assessing the Potential of Photosensitizing Flavoproteins as Tags for
32 Correlative Microscopy. *Chem. Commun.* **2016**, *52*, 8405–8408.
33 <https://doi.org/10.1039/c6cc03119f>.
- 34
35
36
37 (14) Proshkina, G. M.; Shramova, E. I.; Shilova, O. N.; Ryabova, A. V.; Deyev, S. M.
38 Phototoxicity of Flavoprotein MiniSOG Induced by Bioluminescence Resonance
39 Energy Transfer in Genetically Encoded System NanoLuc-MiniSOG Is Comparable
40 with Its LED-Excited Phototoxicity. *J. Photochem. Photobiol. B Biol.* **2018**, *188*, 107–
41 115. <https://doi.org/10.1016/j.jphotobiol.2018.09.006>.
- 42
43
44
45 (15) Souslova, E. A.; Mironova, K. E.; Deyev, S. M. Applications of Genetically Encoded
46 Photosensitizer MiniSOG: From Correlative Light Electron Microscopy to
47 Immunophotosensitizing. *J. Biophotonics* **2017**, *10*, 338–352.
48 <https://doi.org/10.1002/jbio.201600120>.
- 49
50
51
52 (16) Varbanov, H. P.; Jakupec, M. A.; Roller, A.; Jensen, F.; Galanski, M.; Keppler, B.
53 K. Theoretical Investigations and Density Functional Theory Based Quantitative
54 Structure–Activity Relationships Model for Novel Cytotoxic Platinum(IV)
55 Complexes. *J. Med. Chem.* **2013**, *56*, 330–344. <https://doi.org/10.1021/jm3016427>.
- 56
57
58
59 (17) Englinger, B.; Pirker, C.; Heffeter, P.; Terenzi, A.; Kowol, C. R.; Keppler, B. K.;
60

- 1
2 Berger, W. Metal Drugs and the Anticancer Immune Response. *Chem. Rev.* **2019**,
3 *119*, 1519–1624. <https://doi.org/10.1021/acs.chemrev.8b00396>.
- 4
5
6 (18) Weber, S.; Walker, J. M. *Flavins and Flavoproteins IN Series Editor*.
- 7
8 (19) Chaiyen, P.; Fraaije, M. W.; Mattevi, A. The Enigmatic Reaction of Flavins with
9 Oxygen. *Trends Biochem. Sci.* **2012**, *37*, 373–380.
10 <https://doi.org/10.1016/j.tibs.2012.06.005>.
- 11
12 (20) Ghisla, S.; Massey, V.; Lhoste, J.-M.; Mayhew, S. G. Fluorescence and Optical
13 Characteristics of Reduced Flavines and Flavoproteins. *Biochemistry* **1974**, *13*,
14 589–597. <https://doi.org/10.1021/bi00700a029>.
- 15
16 (21) Gargiulo, S.; Arends, I. W. C. E.; Hollmann, F. A Photoenzymatic System for Alcohol
17 Oxidation. *ChemCatChem* **2011**, *3*, 338–342.
18 <https://doi.org/10.1002/cctc.201000317>.
- 19
20 (22) Rauch, M.; Schmidt, S.; Arends, I. W. C. E.; Oppelt, K.; Kara, S.; Hollmann, F.
21 Photobiocatalytic Alcohol Oxidation Using LED Light Sources. *Green Chem.* **2017**,
22 *19*, 376–379. <https://doi.org/10.1039/c6gc02008a>.
- 23
24 (23) Kao, Y.-T.; Saxena, C.; He, T.-F.; Guo, L.; Wang, L.; Sancar, A.; Zhong, D. Ultrafast
25 Dynamics of Flavins in Five Redox States. *J. Am. Chem. Soc.* **2008**, *130*, 13132–
26 13139. <https://doi.org/10.1021/ja8045469>.
- 27
28 (24) Feldmeier, C.; Bartling, H.; Magerl, K.; Gschwind, R. M. LED-Illuminated NMR
29 Studies of Flavin-Catalyzed Photooxidations Reveal Solvent Control of the Electron-
30 Transfer Mechanism. *Angew. Chemie Int. Ed.* **2015**, *54*, 1347–1351.
31 <https://doi.org/10.1002/anie.201409146>.
- 32
33 (25) Bartling, H. Dissertation: NMR Spectroscopic Investigations on Photocatalytic
34 Reactions and Photochromic Materials., Universität Regensburg, 2016.
- 35
36 (26) Cardoso, D. R.; Franco, D. W.; Olsen, K.; Andersen, M. L.; Skibsted, L. H. Reactivity
37 of Bovine Whey Proteins, Peptides, and Amino Acids toward Triplet Riboflavin as
38 Studied by Laser Flash Photolysis. *J. Agric. Food Chem.* **2004**, *52*, 6602–6606.
39 <https://doi.org/10.1021/jf0401165>.
- 40
41 (27) Dabbish, E.; Ponte, F.; Russo, N.; Sicilia, E. Antitumor Platinum(IV) Prodrugs: A
42 Systematic Computational Exploration of Their Reduction Mechanism by L-Ascorbic
43 Acid. *Inorg. Chem.* **2019**, *58*, 3851–3860.
44 <https://doi.org/10.1021/acs.inorgchem.8b03486>.
- 45
46 (28) Torra, J.; Lafaye, C.; Signor, L.; Aumonier, S.; Flors, C.; Shu, X.; Nonell, S.;
47 Gotthard, G.; Royant, A. Tailing MiniSOG: Structural Bases of the Complex
48
49
50
51
52
53
54
55
56
57
58
59
60

- 1
2 Photophysics of a Flavin-Binding Singlet Oxygen Photosensitizing Protein. *Sci.*
3 *Rep.* **2019**, *9*, 2428. <https://doi.org/10.1038/s41598-019-38955-3>.
- 4
5
6 (29) Westberg, M.; Holmegaard, L.; Pimenta, F. M.; Etzerodt, M.; Ogilby, P. R. Rational
7 Design of an Efficient, Genetically Encodable, Protein-Encased Singlet Oxygen
8 Photosensitizer. *J. Am. Chem. Soc.* **2015**, *137*, 1632–1642.
9 <https://doi.org/10.1021/ja511940j>.
- 10
11
12 (30) Pimenta, F. M.; Jensen, R. L.; Breitenbach, T.; Etzerodt, M.; Ogilby, P. R. Oxygen-
13 Dependent Photochemistry and Photophysics of “MiniSOG,” a Protein-Encased
14 Flavin. *Photochem. Photobiol.* **2013**, *89*, 1116–1126.
15 <https://doi.org/10.1111/php.12111>.
- 16
17
18 (31) Silva, A. V.; López-Sánchez, A.; Junqueira, H. C.; Rivas, L.; Baptista, M. S.;
19 Orellana, G. Riboflavin Derivatives for Enhanced Photodynamic Activity against
20 Leishmania Parasites. *Tetrahedron* **2015**, *71*, 457–462.
21 <https://doi.org/10.1016/j.tet.2014.11.072>.
- 22
23
24 (32) Varbanov, H. P.; Valiahdi, S. M.; Kowol, C. R.; Jakupec, M. A.; Galanski, M.;
25 Keppler, B. K. Novel Tetracarboxylatoplatinum(IV) Complexes as Carboplatin
26 Prodrugs. *Dalton. Trans.* **2012**, *41*, 14404–14415.
27 <https://doi.org/10.1039/C2DT31366A>.
- 28
29
30 (33) Gramatica, P.; Papa, E.; Luini, M.; Monti, E.; Gariboldi, M. B.; Ravera, M.; Gabano,
31 E.; Gaviglio, L.; Osella, D. Antiproliferative Pt(IV) Complexes: Synthesis, Biological
32 Activity, and Quantitative Structure–Activity Relationship Modeling. *JBIC J. Biol.*
33 *Inorg. Chem.* **2010**, *15*, 1157–1169. <https://doi.org/10.1007/s00775-010-0676-4>.
- 34
35
36 (34) Tetko, I. V.; Varbanov, H. P.; Galanski, M.; Talmaciu, M.; Platts, J. A.; Ravera, M.;
37 Gabano, E. Prediction of LogP for Pt(II) and Pt(IV) Complexes: Comparison of
38 Statistical and Quantum-Chemistry Based Approaches. *J. Inorg. Biochem.* **2016**,
39 *156*, 1–13. <https://doi.org/https://doi.org/10.1016/j.jinorgbio.2015.12.006>.
- 40
41
42 (35) Jhulki, I.; Chanani, P. K.; Abdelwahed, S. H.; Begley, T. P. A Remarkable Oxidative
43 Cascade That Replaces the Riboflavin C8 Methyl with an Amino Group during
44 Roseoflavin Biosynthesis. *J. Am. Chem. Soc.* **2016**, *138*, 8324–8327.
45 <https://doi.org/10.1021/jacs.6b02469>.
- 46
47
48 (36) Rabello, B. R.; Gerola, A. P.; Pellosi, D. S.; Tessaro, A. L.; Aparício, J. L.; Caetano,
49 W.; Hioka, N. Singlet Oxygen Dosimetry Using Uric Acid as a Chemical Probe:
50 Systematic Evaluation. *J. Photochem. Photobiol. A Chem.* **2012**, *238*, 53–62.
51 <https://doi.org/10.1016/j.jphotochem.2012.04.012>.
- 52
53
54
55
56
57
58
59
60

- 1
2
3
4
5
6
7
8
9
10
11
12
13
14
15
16
17
18
19
20
21
22
23
24
25
26
27
28
29
30
31
32
33
34
35
36
37
38
39
40
41
42
43
44
45
46
47
48
49
50
51
52
53
54
55
56
57
58
59
60
- (37) Gomes, A.; Fernandes, E.; Lima, J. L. F. C. Fluorescence Probes Used for Detection of Reactive Oxygen Species. *J. Biochem. Biophys. Methods* **2005**, *65*, 45–80. <https://doi.org/10.1016/j.jbbm.2005.10.003>.
- (38) Frisch, M. J.; Trucks, G. W.; Schlegel, H. B.; Scuseria, G. E.; Robb, M. A.; Cheeseman, J. R.; Scalmani, G.; Barone, V.; Petersson, G. A.; Nakatsuji, H.; Li, X.; Caricato, M.; Marenich, A. V.; Bloino, J.; Janesko, B. G.; Gomperts, R.; Mennucci, B.; Hratchian, H. P.; Ortiz, J. V.; Izmaylov, A. F.; Sonnenberg, J. L.; Williams-Young, D.; Ding, F.; Lipparini, F.; Egidi, F.; Goings, J.; Peng, B.; Petrone, A.; Henderson, T.; Ranasinghe, D.; Zakrzewski, V. G.; Gao, J.; Rega, N.; Zheng, G.; Liang, W.; Hada, M.; Ehara, M.; Toyota, K.; Fukuda, R.; Hasegawa, J.; Ishida, M.; Nakajima, T.; Honda, Y.; Kitao, O.; Nakai, H.; Vreven, T.; Throssell, K.; Montgomery Jr., J. A.; Peralta, J. E.; Ogliaro, F.; Bearpark, M. J.; Heyd, J. J.; Brothers, E. N.; Kudin, K. N.; Staroverov, V. N.; Keith, T. A.; Kobayashi, R.; Normand, J.; Raghavachari, K.; Rendell, A. P.; Burant, J. C.; Iyengar, S. S.; Tomasi, J.; Cossi, M.; Millam, J. M.; Klene, M.; Adamo, C.; Cammi, R.; Ochterski, J. W.; Martin, R. L.; Morokuma, K.; Farkas, O.; Foresman, J. B.; Fox, D. J. Gaussian 16, Revision B.01. 2016.
- (39) Adamo, C.; Barone, V. Toward Reliable Density Functional Methods without Adjustable Parameters: The PBE0 Model. *J. Chem. Phys.* **1999**, *110*, 6158–6170. <https://doi.org/10.1063/1.478522>.
- (40) Weigend, F.; Ahlrichs, R. Balanced Basis Sets of Split Valence, Triple Zeta Valence and Quadruple Zeta Valence Quality for H to Rn: Design and Assessment of Accuracy. *Phys. Chem. Chem. Phys.* **2005**, *7*, 3297–3305. <https://doi.org/10.1039/B508541A>.
- (41) Grimme, S.; Ehrlich, S.; Goerigk, L. Effect of the Damping Function in Dispersion Corrected Density Functional Theory. *J. Comput. Chem.* **2011**, *32*, 1456–1465. <https://doi.org/10.1002/jcc.21759>.
- (42) Chai, J.-D.; Head-Gordon, M. Long-Range Corrected Hybrid Density Functionals with Damped Atom–Atom Dispersion Corrections. *Phys. Chem. Chem. Phys.* **2008**, *10*, 6615–6620. <https://doi.org/10.1039/B810189B>.
- (43) Zhao, Y.; Truhlar, D. G. The M06 Suite of Density Functionals for Main Group Thermochemistry, Thermochemical Kinetics, Noncovalent Interactions, Excited States, and Transition Elements: Two New Functionals and Systematic Testing of Four M06-Class Functionals and 12 Other Function. *Theor. Chem. Acc.* **2008**, *120*, 215–241. <https://doi.org/10.1007/s00214-007-0310-x>.

- 1
2
3 (44) Reed, A. E.; Curtiss, L. A.; Weinhold, F. Intermolecular Interactions from a Natural
4 Bond Orbital, Donor-Acceptor Viewpoint. *Chem. Rev.* **1988**, *88*, 899–926.
5 <https://doi.org/10.1021/cr00088a005>.
6
7 (45) Chirlan, L. E.; Francl, M. M. Atomic Charges Derived from Electrostatic Potentials:
8 A Detailed Study. *J. Comput. Chem.* **1987**, *8*, 894–905.
9 <https://doi.org/10.1002/jcc.540080616>.
10
11
12
13
14
15
16
17
18
19
20
21
22
23
24
25
26
27
28
29
30
31
32
33
34
35
36
37
38
39
40
41
42
43
44
45
46
47
48
49
50
51
52
53
54
55
56
57
58
59
60